Available online at www.sciencedirect.com
ScienceDirect
Trans. Nonferrous Met. Soc. China 35(2025) 3147−3160
Transactions of Nonferrous Metals Society of China
www.tnmsc.cn

Kinetics study on separation and recovery of In−Pb solder by vacuum volatilization

Jian PANG[1,2,3,4*], Chao-wei DONG[4*], Bao-qiang XU[1,2,3,4], Ling-xin KONG[1,2,3,4], Bin YANG[1,2,3,4]

1. Key Laboratory for Nonferrous Metal Vacuum Metallurgy of Yunnan Province, Kunming University of Science and Technology, Kunming 650093, China;
2. State Key Laboratory of Complex Nonferrous Metal Resources Clean Utilization, Kunming University of Science and Technology, Kunming 650093, China;
3. National Engineering Research Center of Vacuum Metallurgy, Kunming University of Science and Technology, Kunming 650093, China;
4. School of Metallurgical and Energy Engineering, Kunming University of Science and Technology, Kunming 650093, China

Received 24 December 2023; accepted 7 August 2024

Abstract: The vacuum volatilization kinetics of Pb in In−Pb solder was investigated. The results indicate a significant increase in the vacuum volatilization rates of Pb, 25In−75Pb, 40In−60Pb, and In with increasing temperatures from 923 to 1123 K, system pressure of 3 Pa and holding time of 30 min. The mass transfer coefficients and apparent activation energies of Pb and its alloys were determined at various temperatures. Additionally, a kinetics model was developed to describe Pb vacuum volatilization in high-temperature melts. It is obtained that the vapor mass transfer is the factor limiting the vacuum volatilization rates of Pb and In–Pb alloys under the above specified conditions.
Key words: vacuum volatilization; In−Pb alloy; solder; rate equation; kinetics model

1 Introduction

Electronic systems play an indispensable role in diverse sectors, such as industry, agriculture, science, defense, and medicine [1], and thus have become an integral part of modern life. The performance, reliability, and production economics of electronic systems are significantly affected by the solder used in their assembly [2]. In and In-based solders, known for their low melting points, malleability, ductility, and excellent resistance to alkaline corrosion [3,4], exhibit excellent wetting properties on both metallic and nonmetallic substrates. This leads to solder joints with exceptional plasticity and low electrical resistance. Consequently, In-based solders have become the primary choice for assembling microelectronic components [5,6].

Two In−Pb alloys, 25In−75Pb and 40In−60Pb (in wt.%) alloys, are widely used owing to their low melting points of 513 and 447 K, respectively [7]. These alloys exhibit excellent thermal fatigue resistance and wettability properties, preventing gold and silver corrosion, making them highly suitable for preparing gold-plated interfaces. In addition, the 25In−75Pb alloy is easy to process and exhibits robust strength, good thermal stability, and

* Jian PANG and Chao-wei DONG contributed equally to this work
Corresponding author: Ling-xin KONG, Tel: +86-15987180307, E-mail: kkmust@126.com;
Bin YANG, Tel: +86-871-65161583, E-mail: kgyb2005@126.com
https://doi.org/10.1016/S1003-6326(25)66872-5

high reliability, making it ideal for creating superconducting interconnections of multichip arrays within single-flux quantum circuit systems [8]. With the increased disposal of electrical and electronic equipment, the market potential for material recovery has become substantial [9]. Recovering In−Pb solder from discarded electronic products is of significant ecological and economic importance.

Various methods have been proposed for the recovery of In−Pb alloys. WANG et al [10] found an electro-dissolution–extraction technique involving 24 h of electrolytic refinement of the alloy in a silicon fluoride solution, followed by multitier extraction of In from silicon fluoride electrolyte using di(2-ethylhexyl) phosphoric acid to separate In from Pb. ZHANG et al [11] used a leaching solvent extraction method to recover In and Pb from Pb smelting dust, achieving an In recovery rate of over 98% through a process involving dual-stage pressurized sulfuric acid leaching, atmospheric sulfuric acid leaching of the residue, and a three-stage extraction process. Other methods, such as acid/alkali leaching [12] and chlorination [13], have drawbacks, including prolonged duration, inefficiency, waste generation, and environmental hostility. Vacuum volatilization, known for its cleanliness and efficiency, has been widely adopted in alloy separation and resource recovery [14,15]. Thus, the separation and recovery of In−Pb alloy waste via vacuum volatilization appear promising.

Current research on alloy vacuum volatilization primarily focuses on thermodynamics and the effects of temperature, pressure, and time on the efficiency of alloy separation through studies on saturated vapor pressure, separation coefficients, and vapor–liquid equilibrium [16−18]. However, these thermodynamic analyses often overlook the transient states of reactions by focusing only on their initial and final states. The vacuum volatilization of metallic elements is significantly influenced not only by thermodynamic factors but also by kinetic processes. Understanding vacuum metallurgy dynamics is crucial for improving the production efficiency and quality of a product while reducing the energy consumption of the production process. Current research on vacuum metallurgy dynamics is mainly focused on investigating the volatilization of single elements from pure metals or their dilute solutions either under high-temperature and high-vacuum conditions [19,20] or through molecular dynamics simulations [21]. Few experimental and modeling studies have been conducted on the kinetics of alloy vacuum volatilization; the volatilization rate, mechanism, and limiting factors of Pb, In, and In−Pb alloys during vacuum volatilization have not been comprehensively reported.

This study focused on Pb, In, and 25In−75Pb and 40In–60Pb alloys, utilizing the differences in the volatilization characteristics of In and Pb under high-temperature vacuum conditions for the clean and efficient separation and recovery of these two valuable metals. The variations in the volatilization rates of In−Pb alloys with temperature during vacuum volatilization were observed, and an equation to determine the empirical volatilization rate of In−Pb alloys was established. Kinetic parameters, such as the volatilization rate, mass transfer coefficient, and apparent activation energy, of the pure metals and alloys were discussed in detail. The migration mechanism of Pb during the volatilization of Pb and In−Pb alloys was clarified. In addition, a Pb vacuum volatilization kinetics model was developed, pioneering the application of the modified molecular interaction volume model (M-MIVM) to Pb volatilization and mass transfer. The model helped evaluate the factors limiting Pb volatilization. This study aimed to provide foundational theoretical guidance for predicting the optimal temperature and volatilization time for the separation and purification of Pb and In through vacuum distillation.

2 Experimental

2.1 Materials

Pure In and Pb (>99.999%) used in the study were obtained from Yunnan Tin Co., Ltd., and Henan Yuguang Gold Lead Co., Ltd., respectively, and were used as received. The alloys were prepared with In/Pb mass ratios of 25∶75 and 40∶60, designated as 25In−75Pb and 40In−60Pb, respectively.

2.2 Experimental procedures

2.2.1 Alloy melting

After thoroughly mixing the In and Pb alloys

(with In/Pb mass ratios of 25:75 and 40:60) in a graphite crucible (carbon content ≥99.9%, inner diameter: 30 mm, and depth: 25 mm), the mixtures were placed in a custom-fabricated metal-melting apparatus [22]. The apparatus was purged by alternately applying vacuum and Ar gas (purity >99.99%) for five cycles. The temperature (T) was then increased to 723 K under Ar and maintained at that value for 2 h. The material was rapidly cooled in water to complete a single high-temperature melting−quenching cycle. This cycle was repeated thrice to obtain the desired 25In−75Pb and 40In−60Pb alloys.

2.2.2 Volatilization of metals and alloys under vacuum

Figure 1 shows the structure of the vacuum differential thermal weighing furnace used in this study, with a maximum temperature of 2073 K and a minimum system pressure of 0.01 Pa [23]. The pure metals and alloys were placed in a graphite crucible (carbon content >99.9%, inner diameter: 30 mm, and depth: 35 mm) and centrally aligned using an annular heater. A platinum–rhodium thermocouple (range: 273−1873 K and precision: ±1.5 K) was placed above the sample. The furnace pressure was stabilized at 3 Pa using a vacuum pump. The heating system was allowed to uniformly attain a preset temperature within 30 min at a heating rate of 15 K/min. The reduction of the crucible contents was recorded using an analytical balance. The pressure in the vacuum furnace was maintained at (3±0.3) Pa. All materials, including the condensates on the cooling plate and residues within the crucible, were recovered following their cooling to ambient temperature (298 K).

2.3 Determination of elemental contents and their distribution

The morphological characteristics and elemental distribution of the alloys, as well as the volatilized substances remaining after the experiment, were determined using scanning electron microscopy coupled with energy dispersive spectroscopy (SEM−EDS). The In content in the volatilized substances was quantified using inductively coupled plasma optical emission spectrometry (ICP-OES) with a measurement accuracy of 0.0001%.

2.4 Experimental principle

The volatilization rates of the specimens under vacuum were determined using a differential weighing technique by creating a mass-loss curve based on the change in the specimen mass during vacuum volatilization at a specified temperature, system pressure, and volatilization surface area. The true volatilization rate (ω) was calculated using the slope of the linear fit by

$$\omega = \frac{\Delta m}{\Delta t} \cdot \frac{1}{A} = \frac{s}{A} \tag{1}$$

where Δm (g) is the change of mass within Δt, Δt represents the time change (s), A is the volatilization surface area of the melt (7.065 cm^2), and s is the linear fit slope of the mass-loss curve (g/s).

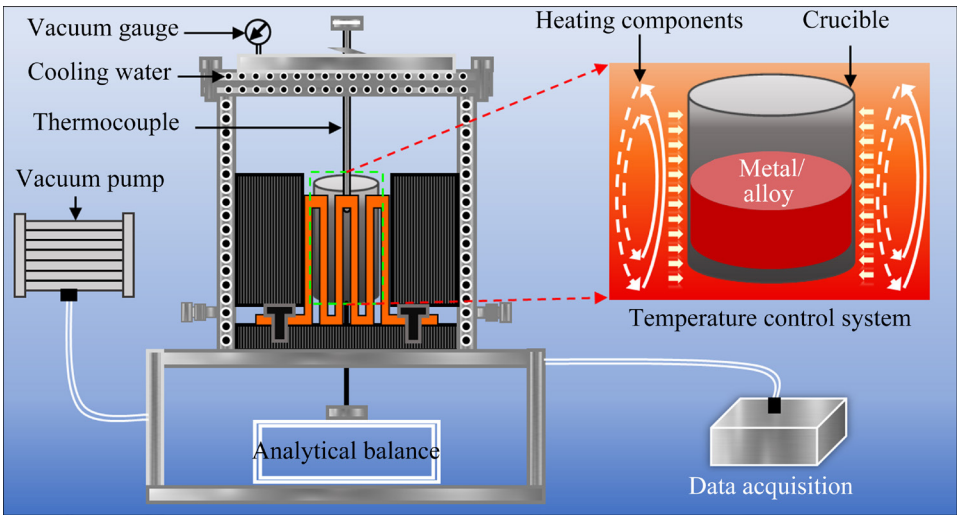

Fig. 1 Structure of vacuum differential thermal weighing furnace

3 Results and discussion

The uniformity of the synthesized alloys before melting was verified using SEM−EDS. As can be seen from Fig. 2, In and Pb were uniformly distributed in the 25In−75Pb and 40In−60Pb alloys.

3.1 Temperature−volatilization rate relationship of In, Pb, and In−Pb alloys

The variation of the volatilization masses of Pb, 25In−75Pb alloy, 40In−60Pb alloy, and In with the holding time (0−1800 s) is shown in Fig. 3 for several temperatures (923, 973, 1023, 1073, and 1123 K). The pressure (3 Pa) and crucible depth

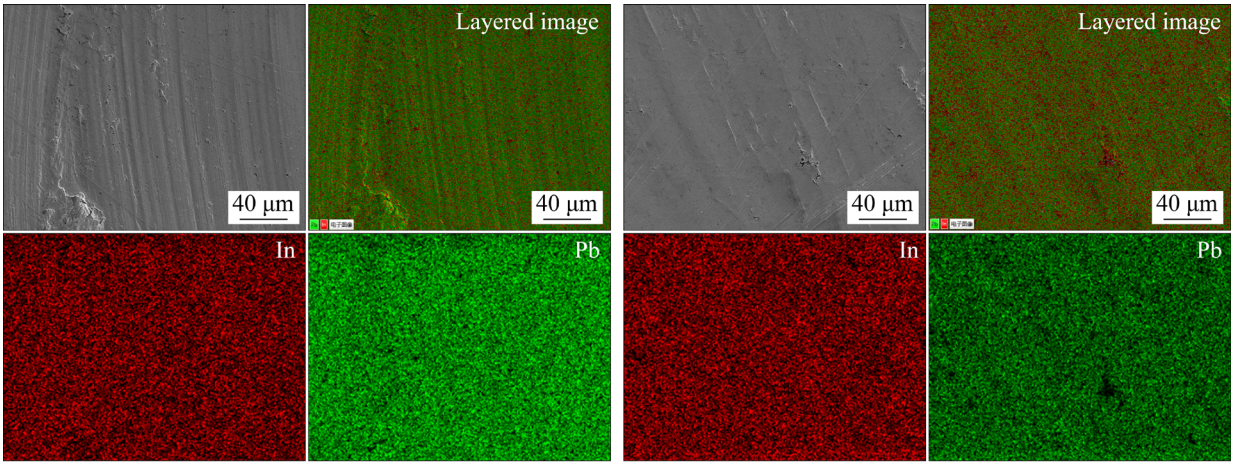

Fig. 2 SEM−EDS images of 25In−75Pb (a) and 40In−60Pb alloys (b)

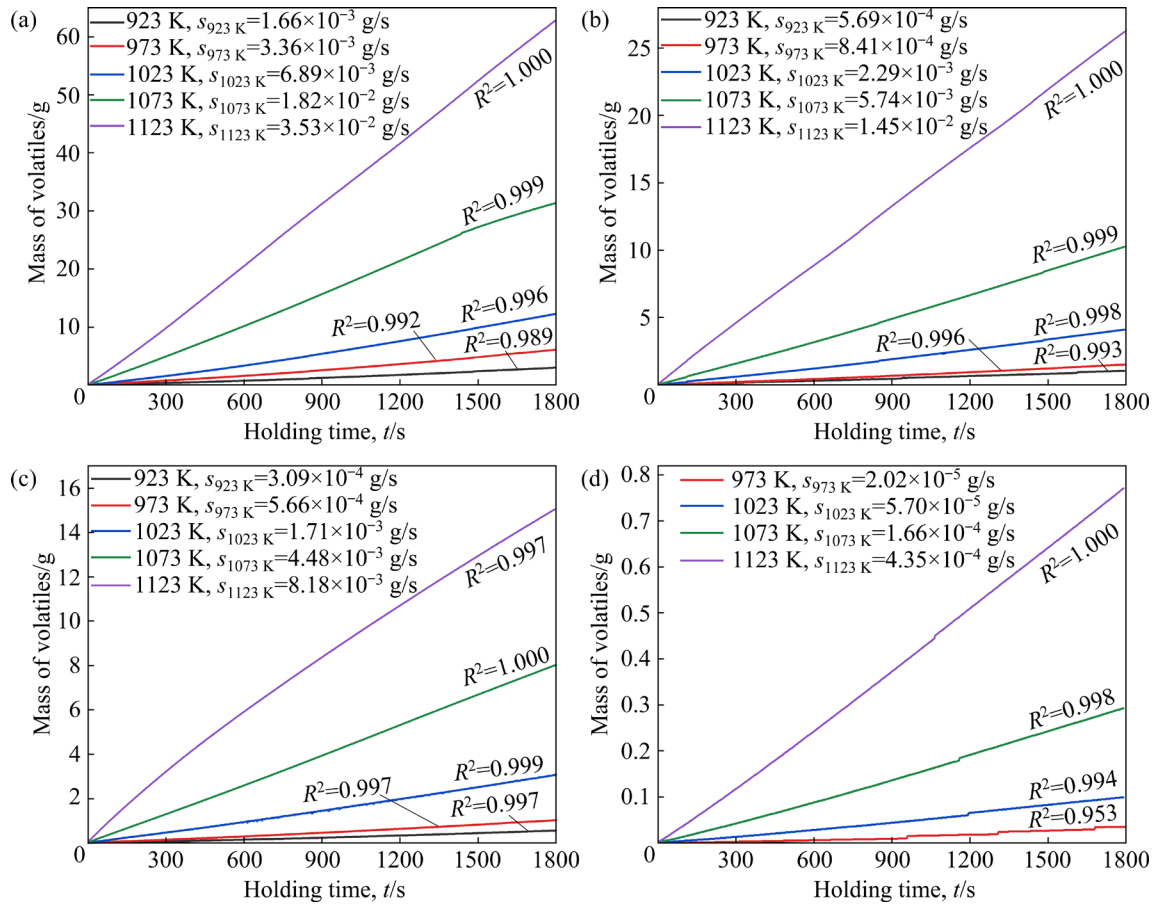

Fig. 3 Relationship between mass of volatiles and holding time for Pb (a), 25In−75Pb alloy (b), 40In−60Pb alloy (c), and In (d) at 3 Pa, h=35 mm and different temperatures

(h=35 mm) were kept unchanged. Linear regression was applied to the volatilization data at various temperatures to extract the s values.

The volatilization masses of Pb, In, 25In−75Pb alloy, and 40In−60Pb alloy increased with increasing temperature, particularly at high temperatures (Fig. 3). For a given temperature, holding time, and pressure, the mass transfer decreased during volatilization as the In content in the specimens increased.

The empirical volatilization rates of Pb, In, 25In−75Pb alloy, and 40In−60Pb alloy, obtained using the s values in Eq. (1) obtained from Fig. 3, demonstrate a significant increase at the same temperature, following the decreasing order of ω_{Pb}> $\omega_{25In-75Pb}$ > $\omega_{40In-60Pb}$ > ω_{In} (Table 1).

The composition of the volatile was determined using ICP-OES. The volatilization rates of Pb and In calculated using Eq. (2) are listed in Table 2.

Table 1 Empirical volatilization rates of Pb, 25In−75Pb alloy, 40In–60Pb alloy, and In

T/K	ω_{Pb}/ ($g\cdot s^{-1}\cdot cm^{-2}$)	$\omega_{25In-75Pb}$/ ($g\cdot s^{-1}\cdot cm^{-2}$)	$\omega_{40In-60Pb}$/ ($g\cdot s^{-1}\cdot cm^{-2}$)	ω_{In}/ ($g\cdot s^{-1}\cdot cm^{-2}$)
923	2.35×10^{-4}	8.05×10^{-5}	4.37×10^{-5}	0
973	4.76×10^{-4}	1.19×10^{-4}	8.01×10^{-5}	2.86×10^{-6}
1023	9.75×10^{-4}	3.24×10^{-4}	2.42×10^{-4}	8.07×10^{-6}
1073	2.58×10^{-3}	8.12×10^{-4}	6.34×10^{-4}	2.35×10^{-5}
1123	5.00×10^{-3}	2.05×10^{-3}	1.16×10^{-3}	6.16×10^{-5}

$$\begin{cases}\omega_{In-Pb}=\omega_{Pb\ in\ In-Pb}+\omega_{In\ in\ In-Pb}\\ \omega_{Pb\ in\ In-Pb}=C_{Pb}\cdot\omega_{In-Pb}\\ \omega_{In\ in\ In-Pb}=C_{In}\cdot\omega_{In-Pb}\end{cases} \quad (2)$$

where ω_{In-Pb} is the In−Pb alloying rate, $\omega_{Pb\ in\ In-Pb}$ and $\omega_{In\ in\ In-Pb}$ denote the individual volatilization rates of Pb and In in the In−Pb alloys, respectively, and C_{Pb} and C_{In} are the elemental contents of Pb and In in the volatiles, respectively.

The volatilization rate of Pb in the In−Pb alloys ($\omega_{Pb\ in\ In-Pb}$) is 11−46 times higher than that of In in the same alloys ($\omega_{In\ in\ In-Pb}$). As the temperature increases, the volatilization ratio of Pb to In decreases, whereas the volatilization rate of In and its volatile content increase. Notably, at a constant temperature, the Pb volatilization rate in the 25In−75Pb alloy was higher than that in the 40In−60Pb alloy.

After vacuum volatilization of the 25In−75Pb and 40In−60Pb alloys at 1123 K, SEM−EDS was used to perform morphological and elemental content analyses of the volatiles (Figs. 4 and 5). The volatiles resulting from the vacuum volatilization of the In−Pb alloys predominantly comprised flakes, stripes, and particles (Figs. 4 and 5). The Pb content in these volatiles varied depending on their morphology, with flakes containing the highest Pb content and stripes having the lowest Pb content.

The actual volatilization rates of Pb, In, 25In−75Pb alloy, and 40In−60Pb alloy (Table 1) were plotted against temperature. Nonlinear fitting employing the Exp2PMod2 model was performed

Table 2 Volatile contents and volatilization rates of Pb−In alloys

Alloy	T/K	Volatile parameter			$\omega_{Pb\ in\ In-Pb}$/ ($g\cdot s^{-1}\cdot cm^{-2}$)	$\omega_{In\ in\ In-Pb}$/ ($g\cdot s^{-1}\cdot cm^{-2}$)
		m/g	C_{Pb}/%	C_{In}/%		
25In–75Pb	923	1.0420	97.88	2.12	7.88×10^{-5}	1.17×10^{-6}
	973	1.5052	97.83	2.17	1.16×10^{-4}	2.58×10^{-6}
	1023	4.1030	97.49	2.51	3.16×10^{-4}	8.14×10^{-6}
	1073	10.2600	96.99	3.01	7.88×10^{-4}	2.45×10^{-5}
	1123	26.2410	95.91	4.09	1.97×10^{-3}	8.39×10^{-5}
40In–60Pb	923	0.5490	96.02	3.98	4.20×10^{-5}	1.74×10^{-7}
	973	1.0130	95.76	4.24	7.67×10^{-5}	3.40×10^{-6}
	1023	3.0570	95.76	4.24	2.32×10^{-4}	1.03×10^{-6}
	1073	8.0080	93.86	6.14	5.95×10^{-4}	3.89×10^{-5}
	1123	15.0460	91.36	8.64	1.06×10^{-3}	1.00×10^{-4}

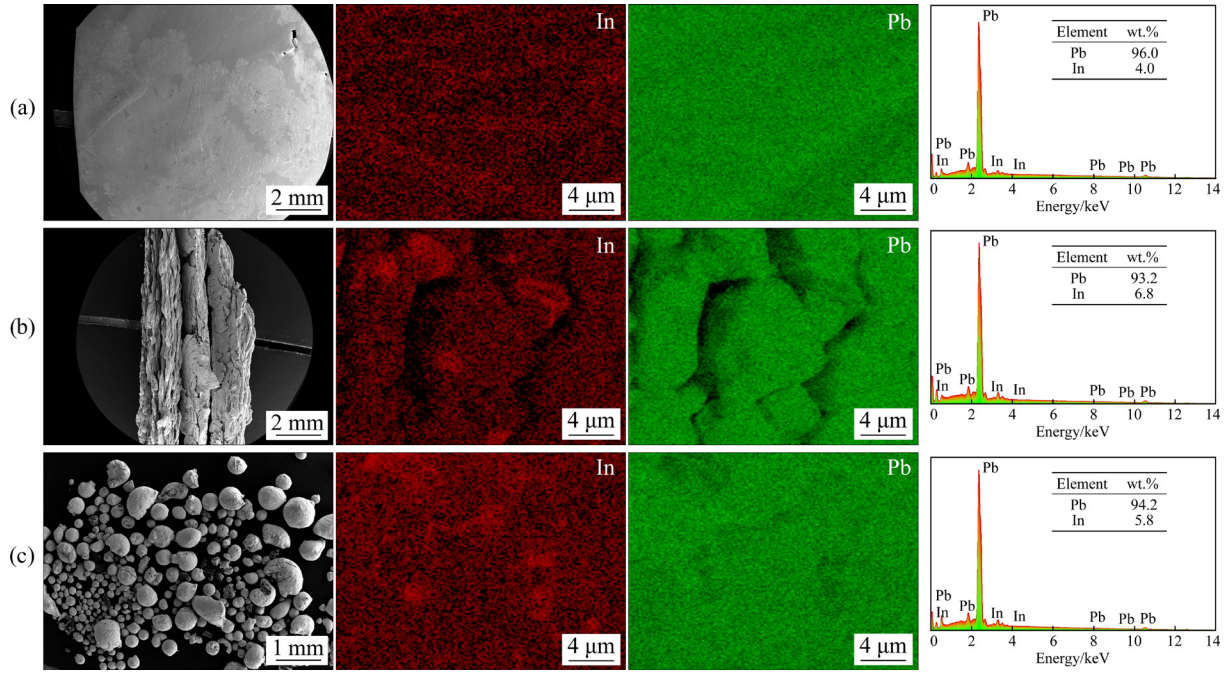

Fig. 4 SEM−EDS analysis results of volatiles in 25In−75Pb alloy at 1123 K, showing flakes (a), stripes (b), and particles (c)

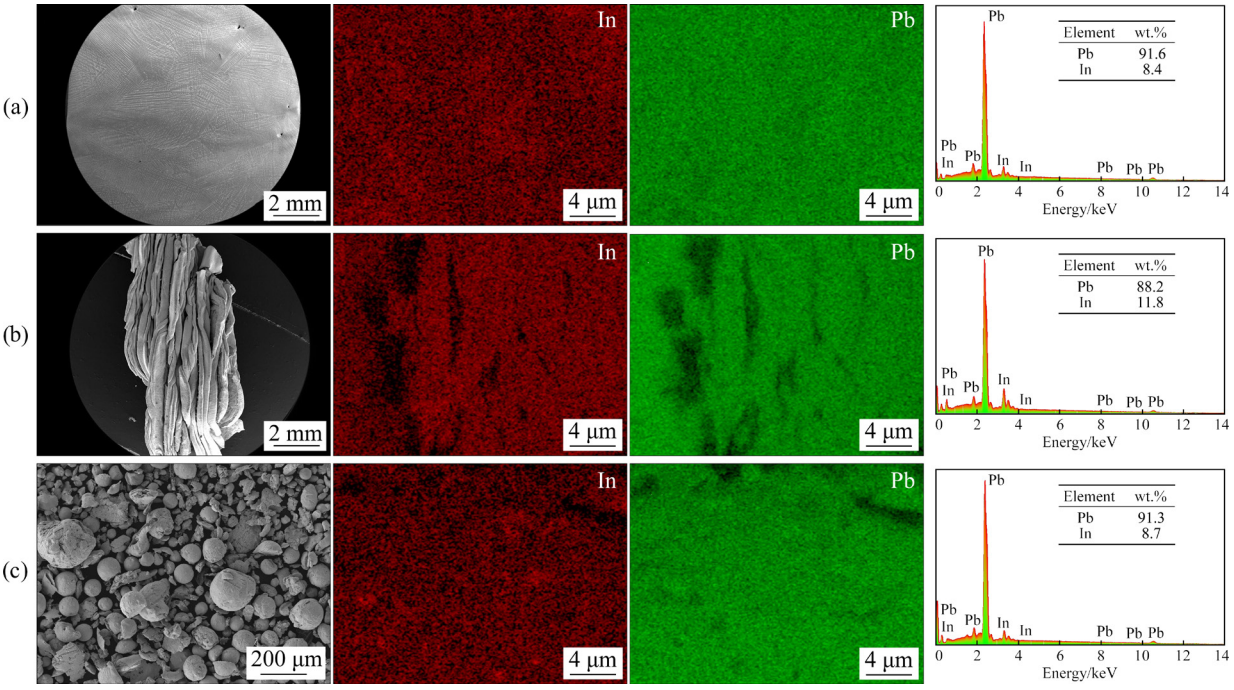

Fig. 5 SEM−EDS analysis results of volatiles in 40In−60Pb alloy at 1123 K, showing flakes (a), stripes (b), and particles (c)

to establish volatilization rate equations for the two pure metals and their alloys (Fig. 6(a)).

Subsequently, the temperature-dependent volatilization rates of Pb and In in the 25In−75Pb and 40In−60Pb alloys were plotted and fitted using the Exp2PMod2 model to derive equations describing the temperature functions of the Pb and In volatilization rates in the In−Pb alloys (Figs. 6(b) and (c)).

The robustness of the fitted volatilization rate equations for the two pure metals and their alloys was confirmed by the square of the correlation

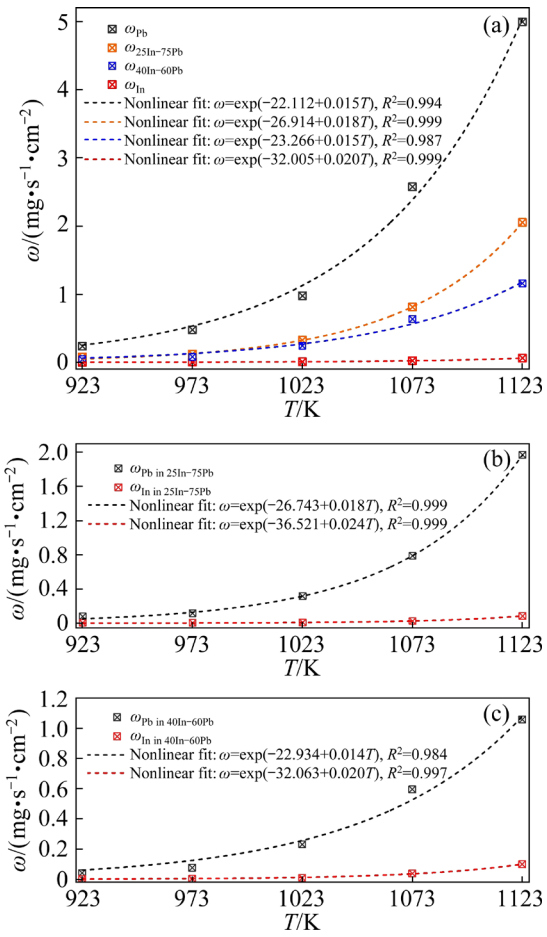

Fig. 6 Distribution of ω of Pb and In in In−Pb (a), 25In−75Pb (b), and 40In−60Pb (c) alloys at 3 Pa, h=35 mm and various temperatures

coefficient (R^2) values, which exceeded 0.98 (Fig. 6), underscoring high reliability of the volatilization rate equations derived. These equations allow the determination of volatilization rates at any temperature within the range of 923−1123 K for a crucible depth of 35 mm, facilitating the design of vacuum volatilization experiments for Pb, In, and In−Pb alloys.

3.2 Temperature−mass transfer coefficient correlation for Pb in In−Pb alloys

The volatilization kinetics for component i, based on kinetic principles, can be described as follows [24]:

$$-\frac{\mathrm{d}C_i(t)}{\mathrm{d}t}=k_i\frac{A}{V}\left(\frac{10^{-7}\rho}{M_i}\right)^{n-1}C_i^n(t) \tag{3}$$

where $C_i(t)$ (mol/L) represents the concentration of element i at time t, k_i is the volatilization rate constant, equivalent to the overall mass transfer coefficient (m/s), V is the melt volume (m^3), n denotes the order of reaction, ρ is the melt density (kg/m^3), and M_i is the molar mass of element i (kg/mol). ρ can be computed as follows:

$$\rho=\rho_m+a(T-T_m) \tag{4}$$

where ρ_m is the metal density at the melting point (T_m); a is the temperature coefficient. T_m, ρ_m and a values of Pb and In are shown in Table 3.

Table 3 T_m, ρ_m, and a of Pb and In

Material	T_m/K	ρ_m/(kg·m^{-3})	a/(kg·m^{-3}·K^{-1})
Pb	600.5	10670	−1.32
In	429.5	7030	−0.68

The density equation for the residual In−Pb alloy melt (ρ_{In-Pb}) can be expressed as

$$\rho_{In-Pb}=w_{Pb,t}\cdot\rho_{Pb,T}+w_{In,t}\cdot\rho_{In,T} \tag{5}$$

where $w_{Pb,t}$ and $w_{In,t}$ are contents (mass fractions) of Pb and In in the melt at time t, respectively; $\rho_{Pb,T}$ and $\rho_{In,T}$ are the liquid densities of Pb and In at temperature T, respectively.

$$V=\frac{m_t}{\rho} \tag{6}$$

where m_t is the melt mass after volatilization at time t.

The reaction order n must be established to determine the overall mass transfer coefficient. Extensive studies [20,24,25] have concluded that vacuum volatilization follows first-order reaction kinetics. Therefore, in this study, we assumed that n=1. By integrating Eq. (3), an alternative representation of the vacuum volatilization kinetics model for the two pure metals and their alloys can be obtained as follows:

$$-\ln\left(\frac{m_t}{m_0}\right)=k_{Pb\ (or\ In)}\frac{A}{V}t\quad\text{(For pure metals)} \tag{7}$$

$$-\ln\left(\frac{w_{Pb,t}}{w_{Pb,0}}\right)=k_{Pb\ in\ In-Pb}\frac{A}{V}t\quad\text{(For alloys)} \tag{8}$$

where m_0 is the melt mass at t=0 s, and $w_{Pb,0}$ is the initial Pb content in the melt at t=0 s. k_{Pb}, k_{In}, and $k_{Pb\ in\ In-Pb}$ represent the overall mass transfer coefficients of Pb, In, and Pb present in the In−Pb alloys, respectively.

The values of ($\ln w_{Pb,0}-\ln w_{Pb,t}$) and ($\ln m_0-\ln m_t$) were obtained using Eqs. (4)−(6). A first-order kinetic reaction approach was adopted in the calculations. After performing linear fitting, the values of ($\ln m_0-\ln m_t$) and ($\ln w_{Pb,0}-\ln w_{Pb,t}$) were plotted against $A\cdot V^{-1}\cdot t$ (Fig. 7). The slope in Fig. 7 reflects the volatile mass transfer coefficient of R^2. The overall mass transfer coefficients are listed in Table 4.

For the first-order reaction kinetics, the relationship between ($\ln w_{Pb,0}-\ln w_{Pb,t}$) and $A\cdot V^{-1}\cdot t$, and that between ($\ln m_0-\ln m_t$) and $A\cdot V^{-1}\cdot t$, exhibit a linear relationship for the two pure metals and their alloys at various temperatures (Fig. 7). Thus, the vacuum volatilization of Pb, In, and In−Pb alloys is governed by a first-order reaction. A positive correlation exists between temperature and the mass transfer coefficient (Table 4). However, as the initial Pb content in the In−Pb alloy melt increased, the mass transfer coefficient of Pb decreased.

3.3 Activation energy for vacuum volatilization

The Arrhenius equation relating the volatilization rate constant k (m/s) to temperature is typically expressed as follows [26]:

$$\ln k = \ln A_1 - \frac{E_a}{RT} \tag{9}$$

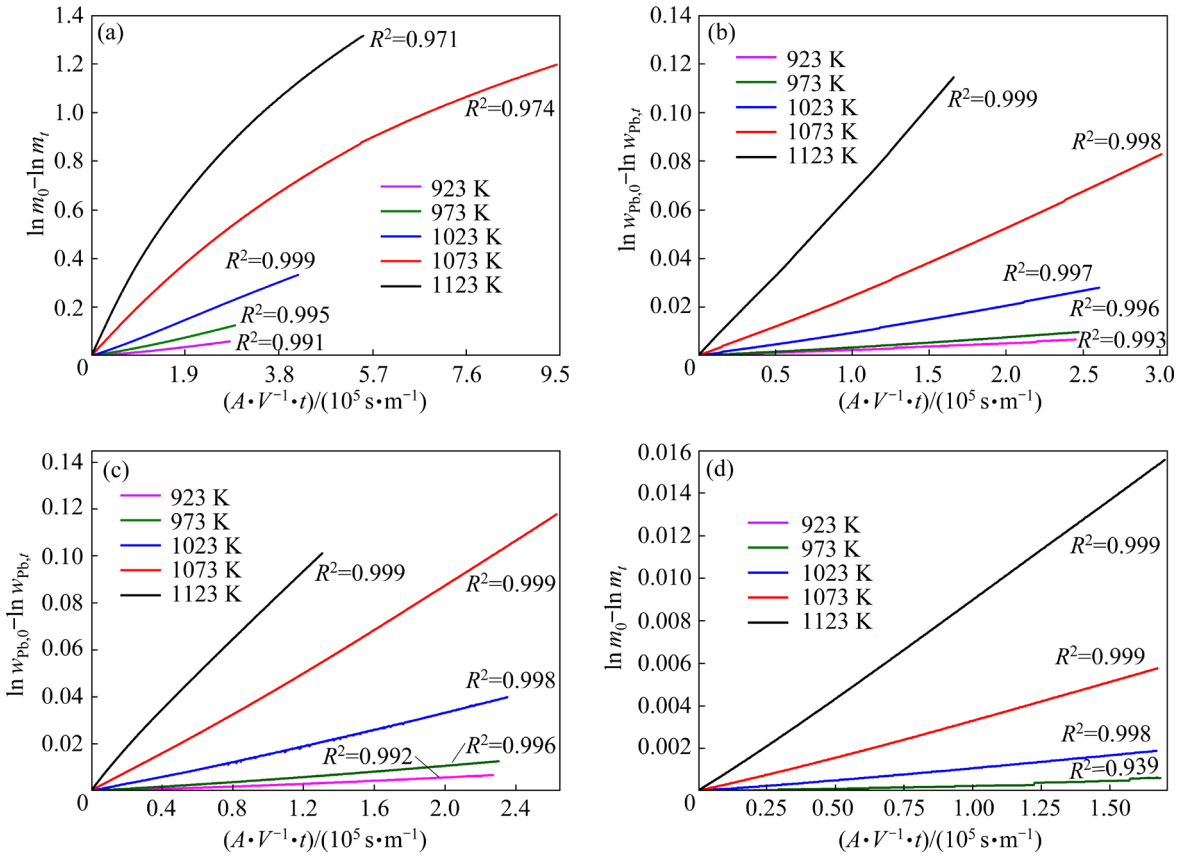

Fig. 7 Plots of ($\ln m_0-\ln m_t$) (a, d) and ($\ln w_{Pb,0}-\ln w_{Pb,t}$) (b, c) against $A\cdot V^{-1}\cdot t$ for Pb (a), 25In−75Pb alloy (b), 40In−60Pb alloy (c), and In (d) for single reaction

Table 4 Mass transfer coefficients of volatile at 3 Pa, h=35 mm and various temperatures

T/K	k_{Pb}/(m·s^{-1})	$k_{Pb\ in\ 25In-75Pb}$/(m·s^{-1})	$k_{Pb\ in\ 40In-60Pb}$/(m·s^{-1})	k_{In}/(m·s^{-1})
923	2.14×10^{-7}	2.64×10^{-8}	2.99×10^{-8}	0
973	4.32×10^{-7}	3.92×10^{-8}	5.49×10^{-8}	3.42×10^{-9}
1023	8.11×10^{-7}	1.07×10^{-7}	1.70×10^{-7}	1.14×10^{-8}
1073	1.35×10^{-6}	2.75×10^{-7}	4.48×10^{-7}	3.47×10^{-8}
1123	2.54×10^{-6}	6.83×10^{-7}	7.60×10^{-7}	9.23×10^{-8}

where A_1 is the pre-exponential factor, representing the product of frequency factors and the probability of a successful reaction; E_a is the activation energy for the vacuum volatilization of pure metals and alloys; R (8.314 J/(mol·K) is the molar gas constant.

As shown in Eq. (9), plotting $\ln k$ against $1/T$ yields a linear graph, with a slope of $-E_a/R$ and an intercept of $\ln A_1$.

The E_a for the volatilization of Pb, 25In−75Pb alloy, 40In−60Pb alloy, and In are 104.95, 144.59, 147.65, and 199.96 kJ/mol, respectively, as shown in Fig. 8. This indicates that as the Pb content in the In−Pb alloys decreases, E_a increases. Therefore, alloys with low initial Pb content require high energy for volatilization during vacuum volatilization.

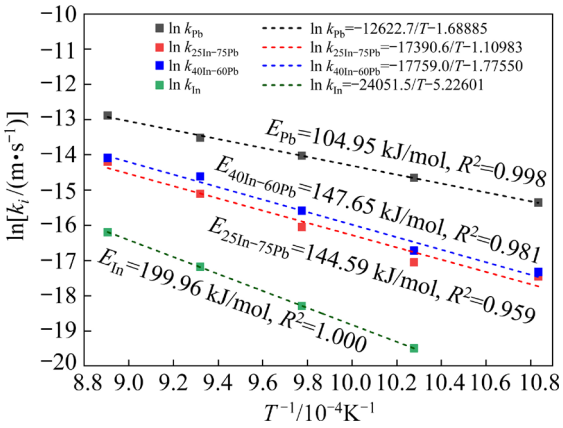

Fig. 8 Relationship between mass transfer coefficient of volatiles and temperature

3.4 Dynamic model for mass transfer and limiting steps in volatilization

The vacuum volatilization of metals occurs at high temperatures and low pressures, necessitating a detailed understanding of the associated mass transfer mechanisms. Figure 9 presents the sequence of mass transfer kinetics of Pb in the In−Pb alloy during volatilization.

The mass transfer sequence can be outlined as follows: Step 1: Diffusion of elements from the liquid phase to the liquid boundary layer; Step 2: Transport of elements across the boundary layer to the melt surface; Step 3: Direct volatilization of the element at the vapor–liquid interface; Step 4: Movement of elements through the vapor boundary layer; Step 5: Combined diffusion and convective mass transfer in the vapor phase; Step 6: Condensation of the elements on the condenser surface.

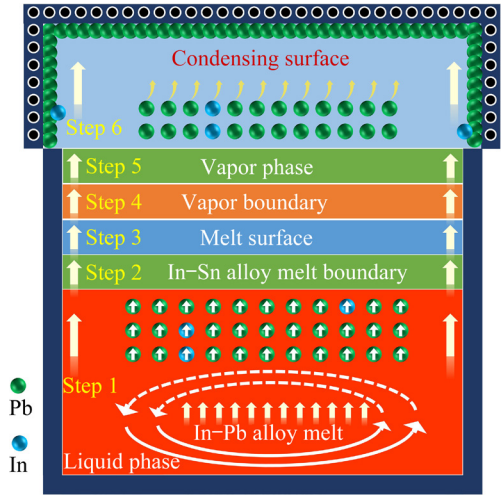

Fig. 9 Schematic of mass transfer during volatilization of In−Pb alloy

The concentration of Pb in the liquid phase and boundary layer is assumed to be uniform, indicating minimal resistance to diffusion or transition across the liquid boundary. Therefore, Steps 1 and 2 are non-rate-limiting. The rapid condensation of Pb vapor, facilitated by a large condensation surface and continuous water cooling, implies that Step 6 is also not rate-limiting. Thus, the rate-determining steps for pure Pb volatilization are a combination of Steps 3−5.

The promotion of rapid atomic diffusion at high temperatures negates the concentration gradient in the liquid phase, rendering Step 1 non-rate-limiting. Similarly, Step 6 is also non-rate-limiting. Therefore, the critical stages associated with In−Pb alloy volatilization could involve only Steps 2−5.

3.4.1 Mass transfer in liquid boundary layer

According to the Machilin model, the molar flux of Pb transferring across the liquid boundary layer to reach the melt surface, denoted as J_i^m (mol/(cm^2·s)), can be calculated as follows [27]:

$$J_i^m = k_i^m (C_i - C_i^s) \quad (10)$$

where C_i is the concentration of component i in the alloy melt (mol/m^3), C_i^s is the concentration of component i in the interface layer between the melt and vapor phase (mol/m^3), and k_i^m is the mass transfer coefficient of component i in the liquid boundary layer (m/s), which is expressed as follows [28]:

$$k_i^{\mathrm{m}}=\sqrt{\frac{8D_i^{\mathrm{m}}v_{\mathrm{m}}}{\pi r_{\mathrm{m}}}} \tag{11}$$

where r_{m} is the melt radius, and v_{m} is the surface flow velocity of the melt. ZHANG [29] indicated that $4.23\times10^{-3}\,\mathrm{m/s}\le v_{\mathrm{m}}\le 1.23\times10^{-2}\,\mathrm{m/s}$ under the vacuum smelting conditions. In this study, v_{m} was considered as $8.27\times10^{-3}\,\mathrm{m/s}$. The diffusion coefficient (D_i^{m}) of component i varies with temperature and the specific type of component in the melt as follows [30]:

$$D_i^{\mathrm{m}}=\frac{k_{\mathrm{B}}T}{4\pi\mu_{\mathrm{In-Pb}}r_i}\left(\frac{M_{\mathrm{Pb}}+M_{\mathrm{In}}}{2M_{\mathrm{Pb}}}\right) \tag{12}$$

where M_{Pb}(=0.2072 kg/mol) is the molar mass of Pb; M_{In}(=0.1148 kg/mol) is the molar mass of In; k_{B}(=1.38×10^{-23} J/K) is the Boltzmann constant; the atomic radius of Pb $r_{\mathrm{Pb}}=1.75\times10^{-10}$ m. The viscosity of the In−Pb alloy melt, $\mu_{\mathrm{In-Pb}}$, is temperature-dependent and can be calculated as [31]

$$\mu_{\mathrm{In-Pb}}=\left(x_{\mathrm{Pb}}\mu_{\mathrm{Pb}}+x_{\mathrm{In}}\mu_{\mathrm{In}}\right)\left(1-2x_{\mathrm{Pb}}x_{\mathrm{In}}\frac{\Delta H}{RT}\right) \tag{13}$$

where ΔH is the enthalpy change of mixing for the In–Pb alloy, obtainable from literature [32]; x_{Pb} and x_{In} are the molar fractions of Pb and In, respectively; μ_{Pb} and μ_{In} are the liquid viscosities of pure Pb and In, respectively, which are calculated by [33]

$$\begin{cases}\mu_{\mathrm{Pb}}=0.5085\exp[8077/(RT)]\\ \mu_{\mathrm{In}}=0.4405\exp[5262/(RT)]\end{cases} \tag{14}$$

By combining Eqs. (11)−(14), k_i^{m} can be obtained.

3.4.2 Mass transfer from melt surface to vapor phase

Based on the studies of Hertz and Langmuir, Knudsen considered the effect of the system pressure on the volatilization rate and derived a theoretical volatilization model, the Hertz−Knudsen−Langmuir equation, to describe the actual volatilization process with enhanced accuracy. This model describes the volatilization of the group element i on the melt surface using the following equation [26]:

$$J_i^{\mathrm{s}}=\frac{x_i^{\mathrm{m}}\gamma_i^{\mathrm{m}}P_i^{*}-x_i^{v}P_{\mathrm{system}}}{\sqrt{2\pi RTM_i}} \tag{15}$$

where J_i^{s} (mol/(cm^2·s)) is the molar flux of Pb volatilized at the vapor–liquid interface; P_i^{*} is the saturation vapor pressure of Pb, which can be obtained using Eq. (16) [34]; x_i^{m} and γ_i^{m} are the molar fraction and activity coefficient of component i in the alloy, respectively; x_i^{v} is the initial molar fraction of component i in the alloy; P_{system} is the system pressure. The analyses presented in Ref. [35] revealed that the M-MIVM accurately predicts the activities and activity coefficients of alloying groups in binary and ternary In-based alloys. Therefore, the M-MIVM was employed to calculate the γ_i^{m} values corresponding to x_i^{m} for various temperatures (Table 5), assuming x_i^{v}, the molar fraction of Pb in the vapor phase, is equal to 1, with Pb being the main component of the vapor phase. The system pressure P_{system} was 3 Pa.

$$\lg P_{\mathrm{Pb}}^{*}=-10130T^{-1}-0.985\lg T+13.28 \tag{16}$$

When the liquid and vapor were under the same constant-temperature conditions, the vacuum volatilization of pure Pb and Pb obtained from the alloys was considered a reversible reaction.

Considering the nature of the kinetics on the liquid surface [36], the molar flux of Pb at the liquid–vapor interface during chemical vaporization can be expressed as follows:

$$J_i^{\mathrm{s}}=k_i^{\mathrm{s}}\frac{\rho}{M_i}\left(1-\frac{P_{\mathrm{system}}}{\alpha P_i^{*}}\right) \tag{17}$$

where k_i^{s} (m/s) is the mass transfer coefficient at the vapor–liquid interface; α is the coefficient of concentration. For pure metals, α=1, and for alloys, $\alpha=x_i^{\mathrm{m}}\cdot\gamma_i^{\mathrm{m}}$. By substituting these values into Eq. (17), k_i^{s} can be calculated by

Table 5 Activity coefficients of Pb in In−Pb alloys at various temperatures

Alloy	$x_{\mathrm{Pb}}^{\mathrm{m}}$	$\gamma_{\mathrm{Pb}}^{\mathrm{m}}$				
		923 K	973 K	1023 K	1073 K	1123 K
25In−75Pb	0.8441	1.0080	1.0075	1.0071	1.0067	1.0063
40In−60Pb	0.7302	1.0249	1.0234	1.0221	1.0209	1.0198

$$k_i^{\mathrm{s}}=\frac{x_i^{\mathrm{m}}\gamma_i^{\mathrm{m}}P_i^{*}}{\rho}\sqrt{\frac{M_i}{2\pi RT}} \tag{18}$$

3.4.3 Mass transfer in vapor boundary layer

The mass transfer coefficient in the vapor boundary layer (k_i^{gb}) [37] can be derived as

$$k_i^{\mathrm{gb}}=\sqrt{\frac{RT_i}{2\pi M_i}} \tag{19}$$

3.4.4 Diffusive and convective mass transfer in vapor phase

The total molar mass transfer flux of component i in the vapor phase is due to both diffusion and convective mass transfer. Once Pb vaporizes from the alloy melt surface into the vapor phase, the total molar mass transfer flux can be expressed as follows (J_i^{g}) [38]:

$$J_i^{\mathrm{g}}=-\frac{D_i^{\mathrm{g}}}{RT}\cdot\frac{\mathrm{d}P_i^{\mathrm{s}}}{\mathrm{d}x}+\frac{v_{i,\mathrm{g}}}{RT}\left(P_i^{\mathrm{e}}-P_i^{\mathrm{s}}\right)=k_i^{\mathrm{g}}C_i^{\mathrm{s}} \tag{20}$$

where D_i^{g} is the diffusion coefficient of component i in the vapor phase (m^2/s), x is the vertical distance to the alloy melt surface (m); P_i^{s} is the partial pressure of component i in the vapor-phase body (Pa); $v_{i,\mathrm{g}}$ is the velocity of component i in vapor flow (m/s); P_i^{e} is the partial pressure of component i on the surface of the solute (Pa); k_i^{g} (m/s^{-1}) is the mass transfer coefficient of component i through the vapor-phase boundary layer. Various simplifications have been proposed for the total molar mass transfer flux J_i^{g} [20,39,40]. However, these simplifications typically result in significant deviations in the theoretical calculations of k_i^{g}. Therefore, in this study, k_i^{g} was calculated based on the experimentally obtained total mass transfer coefficient ($k_{\mathrm{Pb\ in\ In-Pb}}$ or k_{Pb}) (Table 6) using Eqs. (21) and (22), respectively.

$k_{\mathrm{Pb\ in\ In-Pb}}$ can be obtained by

$$\frac{1}{k_{\mathrm{Pb\ in\ In-Pb}}}=\frac{1}{k_i^{\mathrm{m}}}+\frac{1}{k_i^{\mathrm{s}}}+\frac{1}{k_i^{\mathrm{gb}}}+\frac{1}{k_i^{\mathrm{g}}} \tag{21}$$

k_{Pb} can be obtained from by

$$\frac{1}{k_{\mathrm{Pb}}}=\frac{1}{k_i^{\mathrm{s}}}+\frac{1}{k_i^{\mathrm{gb}}}+\frac{1}{k_i^{\mathrm{g}}} \tag{22}$$

3.4.5 Evaluation of limiting steps of mass transfer during vacuum volatilization

The mass transfer coefficients were calculated for different steps involved in mass transfer during vacuum volatilization, based on the theoretical mass transfer model used for Pb volatilization.

An increase in temperature enhanced each mass transfer step, specifically at the vapor–liquid interface and during the diffusive/convective mass transfer of Pb vapor in the vapor phase (Table 6). Conversely, an increase in Pb content in the In−Pb

Table 6 Mass transfer coefficients of Pb volatilization calculated for each mass transfer step

System	T/K	h/mm	k_i^{m}/(m·s^{-1})	k_i^{s}/(m·s^{-1})	k_i^{gb}/(m·s^{-1})	k_i^{g}/(m·s^{-1})
Pb	923	35	−	1.49×10^{-6}	77	2.50×10^{-7}
	973	35	−	5.21×10^{-6}	79	4.71×10^{-7}
	1023	35	−	1.61×10^{-5}	81	8.54×10^{-7}
	1073	35	−	4.48×10^{-5}	83	1.39×10^{-6}
	1123	35	−	1.14×10^{-4}	85	2.60×10^{-6}
25In−75Pb	923	35	2.23×10^{-6}	1.84×10^{-6}	77	2.71×10^{-8}
	973	35	2.36×10^{-6}	6.35×10^{-6}	79	4.01×10^{-8}
	1023	35	2.48×10^{-6}	1.93×10^{-5}	81	1.12×10^{-7}
	1073	35	2.60×10^{-6}	5.31×10^{-5}	83	3.09×10^{-7}
	1123	35	2.72×10^{-6}	1.33×10^{-4}	85	9.18×10^{-7}
40In−60Pb	923	35	2.34×10^{-6}	1.58×10^{-6}	77	3.09×10^{-8}
	973	35	2.47×10^{-6}	5.46×10^{-6}	79	5.67×10^{-8}
	1023	35	2.60×10^{-6}	1.67×10^{-5}	81	1.84×10^{-7}
	1073	35	2.72×10^{-6}	4.60×10^{-5}	83	5.42×10^{-7}
	1123	35	2.85×10^{-6}	1.16×10^{-4}	85	1.05×10^{-6}

alloy decreased mass transfer in the liquid boundary layer, volatilization at the interface, and diffusive or convective mass transfer in the vapor phase. Therefore, the volatilization processes of Pb and In−Pb alloys are predominantly governed by vapor phase mass transfer at temperatures ranging from 923 to 1123 K and a pressure of 3 Pa.

4 Conclusions

(1) The empirical equation for calculating the volatilization rates of Pb, In, In−Pb alloys, and Pb in the In−Pb alloys was obtained. Increasing the Pb content in the In−Pb alloys and the temperature significantly accelerated Pb volatilization.

(2) The volatilization of Pb from the melt followed first-order reaction kinetics. An increase in temperature increased the mass transfer coefficients, whereas a higher initial Pb content resulted in a lower Pb volatilization coefficient.

(3) The apparent activation energies obtained for the vacuum volatilization of Pb, 25In−75Pb alloy, 40In−60Pb alloy, and In were 104.95, 144.59, 147.65, and 199.96 kJ/mol, respectively.

(4) A dynamic model for Pb volatilization was established, revealing that vapor mass transfer was the rate-limiting factor in the vacuum volatilization of both pure metals and their alloys.

CRediT authorship contribution statement

Jian PANG: Conceptualization, Methodology, Investigation, Writing − Original draft, Review and editing; **Chao-wei DONG:** Conceptualization, Methodology, Investigation, Writing − Review and editing; **Bao-qiang XU:** Investigation; **Ling-xin KONG** and **Bin YANG:** Conceptualization, Methodology.

Declaration of competing interest

The authors declare that they have no known competing financial interests or personal relationships that could have appeared to influence the work reported in this paper.

Acknowledgments

This study was financially supported by the Fundamental Research Project of Yunnan Province, China (Nos. 202301AW070020, 202201AT070229, 202105AC160091, 202202AB080018).

References

[1] ZHONG Su-juan, ZHANG Liang, LI Mu-lan, LONG Wei-min, WANG Feng-jiang. Development of lead-free interconnection materials in the electronic industry during the past decades: Structure and properties [J]. Materials & Design, 2022, 215: 110439.

[2] WU Ming, WANG Shan-lin, YIN Li-meng, CHEN Yu-hua, HONG Min, SUN Wen-jun, YAO Zong-xiang, NI Jia-ming, LU Peng, ZHANG Ti-ming, XIE Ji-lin. Oxidation behavior and intermetallic compound growth dynamics of SAC305/Cu solder joints under rapid thermal shock [J]. Transactions of the Nonferrous Metals Society of China, 2023, 33(10): 3054−3066.

[3] TIAN Qing-hua, DONG Bo, GUO Xue-yi, LI Dong, LI Zou-jiang, XU Zhi-peng. Purification of crude indium by two-stage cyclone electrowinning [J]. Transactions of the Nonferrous Metals Society of China, 2023, 33(10): 3185−3197.

[4] LI Cun-xiong, ZHANG Zhao-yan, ZHANG Yao-yang, DENG Zhi-gan, JI Wen-bin, LIN Xiao-tan. Reductive leaching kinetics of indium and further selective separation by fraction precipitation [J]. Transactions of Nonferrous Metals Society of China, 2023, 33(1): 315−324.

[5] LI J F, MANNAN S M, CLODE M P, JOHNSTON C, CROSSLEY A. Dissolution and interfacial reaction of Nb in contact with the molten 52In−48Sn solder [J]. Acta Materialia, 2007, 55(15): 5057−5071.

[6] DESHPANDE M C, CHAUDHARI R, NARAYANAN R, KALE H. Study of mechanical properties of indium-based solder alloys for cryogenic applications [J]. Soldering & Surface Mount Technology, 2022, 34(4): 212−221.

[7] DUKAROV S V, PETRUSHENKO S I, SAMSONIK A L, SUKHOV V N. Phase diagram of In−Pb alloy in condensed films [J]. Physica Status Solidi (a), 2021, 218(2): 2000455.

[8] XU Gao-wei, ZHOU Quan, GAI Wei, WU Yan-hong, REN Jie, WANG Zhen, XIE Xiao-ming LUO Le. A novel superconducting interconnection for superconducting MCM using wire bonding method with Pb−In alloy [C]// Proceedings of the 21st International Conference on Electronic Packaging Technology (ICEPT). Guangzhou: China, 2020: 1−4.

[9] ZHANG Lin-gen, XU Zhen-ming. A review of current progress of recycling technologies for metals from waste electrical and electronic equipment [J]. Journal of Cleaner Production, 2016, 127: 19−36.

[10] WANG Rui-xiang, HE Jing, ZHANG Peng, LIU Wei, ZHANG Wen-hai. Study on recovery of indium from lead alloy bearing indium [J]. Non-feerous Metals (Extractive metallurgy), 2008(1): 26−29. (in Chinese)

[11] ZHANG Yu-hui, JIN Bing-jie, MA Bao-zhong, FENG Xiao-yan. Separation of indium from lead smelting hazardous dust via leaching and solvent extraction [J]. Journal of Environmental Chemical Engineering, 2017, 5(3): 2182−2188.

[12] BARAKAT M A. Recovery of lead, tin, and indium from alloy wire scrap [J]. Hydrometallurgy, 1998, 49: 63−73.

[13] TERAKADO O, ISHIKAWA H, HIRASAWA M. Indium recovery from bearing alloy via pyrometallurgical chlorination process utilizing ammonium chloride [J]. Materials Transactions, 2013, 54(12): 2271−2275.

[14] ZHA Guo-zheng, YANG Chong-fang, WANG Yun-ke, GUO Xin-yu, JIANG Wen-long, YANG Bin. New vacuum distillation technology for separating and recovering valuable metals from a high value-added waste [J]. Separation and Purification Technology, 2019, 209: 863−869.

[15] YANG Bin, HUANG Da-xin, LIU Da-chun, ZHA Guo-zheng, JIANG Wen-long, KONG Xiang-feng. Research and industrial application of a vacuum separation technique for recovering valuable metals from copper dross [J]. Separation and Purification Technology, 2020, 236: 116309.

[16] PANG Jian, WU Hai, KONG Ling-xin, XU Jun-jie, XU Bao-qiang, YANG Bin. Vacuum distillation: A sustainable separation and purification approach for extracting valuable metals from In−Zn, In−Sn, and In−Sn−Zn waste alloys [J]. Separation and Purification Technology, 2024, 330: 125166.

[17] WANG Shuang-ping, ZHAO Jin-yang, XU Bao-qiang, KONG Ling-xin, JIANG Wen-long, YANG Bin. Theoretical research on vacuum separation of Au−Ag alloy [J]. Transactions of Nonferrous Metals Society of China, 2022, 32(8): 2719−2726.

[18] HUANG Da-xin, JIANG Wen-long, XU Bao-qiang, ZHA Guo-zheng, YANG Bin. Purification of metallurgical-grade crude tellurium based on viscous distillation and gas-phase separation [J]. Transactions of Nonferrous Metals Society of China, 2024, 34: 1037−1048.

[19] MITRAŠINOVIĆ A M, ODANOVIĆ Z. Thermodynamic and kinetics investigation of elemental evaporation from molten Al7Si4Cu alloy [J]. Thermochimica Acta, 2021, 695: 178816.

[20] CHU Jian-hua, BAO Yan-ping, LI Xin, WANG Min, GAO Fang. Kinetic study of Mn vacuum evaporation from Mn steel melts [J]. Separation and Purification Technology, 2021, 255: 117698.

[21] SONG Bing-yi, JIANG Wen-long, YANG Bin, CHEN Xiu-min, XU Bao-qiang, KONG Ling-xin, LIU Da-chun, DAI Yong-nian. Study on exploration of azeotropic point of Pb−Sb alloys by vacuum distillation and ab initio molecular dynamic simulation [J]. Metallurgical and Materials Transactions A—Physical Metallurgy and Materials Science, 2016, 47(10): 5214−5222.

[22] PANG Jian, WU Hai, KONG Ling-xin, XU Bao-qiang, XU Jun-jie, YANG Bin. Clean and efficient recovery of In−Sn and In−Sn−Bi lead-free brazing materials by vacuum volatilization and thermodynamic modeling [J]. Vacuum, 2023, 214: 112172.

[23] GUO Xin-yu, ZHAO Yun, ZHA Guo-zheng, WANG Jia-hao, JIANG Wen-long, YANG Bin, MA Wen-hui. Research on the evaporation law of elemental antimony under vacuum [J]. Vacuum, 2022, 200: 110985.

[24] YOU Yan-jun, XU Jun-jie, KONG Ling-xin, XU Bao-qiang, YANG Bin. Kinetics study of Pb evaporation from pure Pb and Pb−Ag alloy in the vacuum evaporation process [J]. Journal of Materials Research and Technology, 2021, 15: 7012−7021.

[25] ZHAO Jin-yang, YANG Hong-wei, NAN Chang-bin, YANG Bin, LIU Da-chun, XU Bao-qiang. Kinetics of Pb evaporation from Pb−Sn liquid alloy in vacuum distillation [J]. Vacuum, 2017, 141: 10−14.

[26] HOSEINPUR A, TANG K, SAFARIAN J. Kinetic study of vacuum evaporation of elements from ternary melts; case of dilute solution of P in Si−Al melts [J]. Separation and Purification Technology, 2020, 235: 116284.

[27] MACHLIN E S. Kinetics of vacuum induction refining theory [J]. Transactions of the American Institute of Mining and Metallurgical Engineers, 1960, 218: 314−326.

[28] JIANG Da-chuan, REN Shi-qiang, SHI Shuang, DONG Wei, QIU Jie-shan, TAN Yi, LI Jia-yan. Phosphorus removal from silicon by vacuum refining and directional solidification [J]. Journal of Electronic Materials, 2014, 43(2): 314−319.

[29] ZHANG Lei. Distribution models of impurities in terbium metal purified by vacuum distillation [D]. Beijing: Beijing General Research Institute for Nonferrous Metals, 2020. (in Chinese)

[30] ENGH T A. SIMENSEN C J, WIJK O. Principles of metal refining [M]. Oxford: Oxford University Press, 1992.

[31] RIALLAND J F, PERRON J C. Viscosities of indium−lead liquid alloys [J]. Metallurgical Transactions, 1974, 5: 2401−2403.

[32] TERZIEFF P. The viscosity of liquid alloys [J]. Journal of Alloys and Compounds, 2008, 453: 233−240.

[33] TAO Dong-ping. The properties of liquid alloys and molten slags — Theory, model, and calculation [M]. Kunming: Yunnan Science and Technology Press, 1997. (in Chinese)

[34] YANG Bin, XU Bao-qiang. Vacuum metallurgy [M]. Changsha: Central South University Press, 2021. (in Chinese)

[35] DAI Heng, TAO Dong-ping. Application of the modified molecular interaction volume model (M-MIVM) to vapor−liquid phase equilibrium of binary alloys in vacuum distillation [J]. Vacuum, 2019, 163: 342−351.

[36] VLASOV V A. Modeling of evaporation and condensation processes: A chemical kinetics approach [J]. Heat and Mass Transfer, 2019, 55(6): 1661−1669.

[37] HUA Yi-xin. Introduction to metallurgical process dynamics [M]. Beijing: Beijing University of Technology Press, 2004. (in Chinese)

[38] HARRIS R, DAVENPORT W G. Vacuum distillation of liquid metals: Part I. Theory and experimental study [J]. Metallurgical and Materials Transactions B: Process Metallurgy and Materials Processing Science, 1982, 13(4): 581−588.

[39] SHI S, LI P T, MENG J X, JIANG D C, TAN Y, ASGHAR H M N U K. Kinetics of volatile impurity removal from silicon by electron beam melting for photovoltaic applications [J]. Physical Chemistry Chemical Physics, 2017, 19(41): 28424−28433.

[40] SAFARIAN J, TANGSTAD M. Vacuum refining of molten silicon [J]. Metallurgical and Materials Transactions B: Process Metallurgy and Materials Processing Science, 2012, 43(6): 1427−1445.

真空挥发分离回收铟铅合金焊料的动力学研究

庞 佺[1,2,3,4]，董超威[4]，徐宝强[1,2,3,4]，孔令鑫[1,2,3,4]，杨 斌[1,2,3,4]

1. 昆明理工大学 云南省有色金属真空冶金重点实验室，昆明 650093；
2. 昆明理工大学 省部共建复杂有色金属资源清洁利用国家重点实验室，昆明 650093；
3. 昆明理工大学 真空冶金国家工程研究中心，昆明 650093；
4. 昆明理工大学 冶金与能源工程学院，昆明 650093

摘 要：研究了铟铅合金钎料中 Pb 的真空挥发动力学。结果表明，在温度为 923~1123 K、系统压力为 3 Pa 及保温时间为 30 min 的条件下，Pb、25In−75Pb、40In−60Pb 和 In 的真空挥发速率随温度的升高而显著增大。获得了 Pb 及其合金在不同温度下的传质系数和表观活化能。此外，构建了高温熔体中 Pb 真空挥发的动力学模型。在以上条件下，气相传质是影响 Pb 和 In−Pb 合金真空挥发的关键因素。

关键词：真空挥发；铟铅合金；焊料；速率方程；动力学模型

(Edited by Wei-ping CHEN)